# Efficient Power Management and Control Strategy of Hybrid Renewable Energy System in Microgrid

J. VINOTHKUMAR[1*], R. THAMIZHSELVAN[2]
[1]Annamalai University, Department of Electrical Engineering, Chidambaram, Tamil Nadu, INDIA
[2]Annamalai University, Department of Electrical Engineering, Chidambaram, Tamil Nadu, INDIA

Abstract: Currently, the use of renewable energy has gradually increased due to the environmental problems present nowadays. The intermittency of distributed renewable generation poses significant challenges for the operation and integration of microgrids. Unlike the main power grid, where load balancing resources, in general, are abundant, the balancing of generation and load in a microgrid must be done by small gas turbines, diesel generators, or energy storage devices with very limited capacity and at much higher costs. Consequently, the proposed methodology seeks a model for minimizing the Energy Cost (EC) and enhancing the power supply for rural areas by designing and analyzing four different hybrid system configurations based on integrating a biomass system with a photovoltaic (PV), wind turbine (WT) and battery system. To ensure the desired power demand with minimum production cost, the research proposed an energy-efficient Hybrid DC/AC microgrid using four renewable energy sources. Lithium-ion batteries were chosen for this study due to their high energy density, long life cycle, and high efficiency. The existence of both AC and DC microgrids has led to a new concept of hybrid AC/DC microgrids which consists of both AC and DC grids tied by an Interlinking Converter (ILC). It comprises a DC grid and AC grid interlinked by a bidirectional DC/AC converter. Such a hybrid AC/DC microgrid has the advantages of both AC and DC with increased efficiency and less cost. To provide higher voltages, the Multi-Input Booster (MIB) DC-DC converters are used as a power converter in between load and source to enforce and increase the PV depending on the voltage output signal. Further extract maximum power from the solar PV system, perturb and observe algorithm-based power point tracking control mechanism is proposed DC link voltage of ILC is regulated usually by DC side control in load sharing among sources in the DC microgrid. In addition, to overcome the load fluctuation problem in a microgrid, the research introduced a Mamdani type 2 PID-fuzzy controller. Performance index parameters of the transient response characteristics are also improved by using the proposed control approach. The time-domain dynamic responses reveal that the proposed type-II fuzzy PID controller can balance the power generation and demand properly and control both system frequency and tie-line power effectively.

Keywords: Microgrid, Photovoltaic, Battery, Wind, Interlinking Converter, Multi-Input Booster, Mamdani type 2 PID-fuzzy controller.

Received: September 29, 2022. Revised: May 28, 2023. Accepted: June 23, 2023. Published: July 17, 2023.

## 1. Introduction

When compared to traditional techniques, using renewable resources to generate power will help to maintain the local environment while also lowering the cost of production. The construction of a hybrid microgrid (MG), which includes wind, solar, power converters, storage devices, and diesel engines has proven to be a viable alternative for supplying energy to isolated places [1]. MG systems with integrated Renewable Energy Sources (RESs) such as solar and wind are becoming more attractive and prevalent in the era of fast-growing green energy technology. Moreover, due to the unpredictable nature of RES power output, battery storage systems have proven to be an inseparable

aspect of MGs, improving the whole system's reliability, efficacy, and operational cost [2]. Hybrid RESs provide several advantages, including the capacity to use a variety of energy sources to serve the community, increasing the penetration of RES while reducing the usage of fossil fuels, and ensuring reliability. Nevertheless, cost, dependability, and electrical efficiency are still significant issues that require further attention. As a result, it's critical to use optimization approaches to improve Hybrid RES performance under different environmental circumstances [3-4].

Several applications were utilized in grids as a result of the introduction of new technology such as microprocessor systems and developments in power electronics, particularly in the creation of controllers and converters [5]. They include solar, fuel cells, wind, small diesel generators, small hydropower, backup energy system and DC/AC load system for consumption of energy. It's difficult to operate to design a hybrid system with all of the renewable and non-RES sources, storage devices, converters, and loads. The hybrid system's DC components are the wind turbine, solar panels, and battery bank, while the AC components are the diesel generator and load. The conversion of AC to DC and vice versa is handled using an IGBT-based high-power converter [6]. Constant power loads (CPLs) in DC MGs diminish the DC-DC converter's effective damping and may have destabilizing effects since CPLs have nonlinear dynamics and negative incremental impedance [7-8]. An MG can be either DC or a hybrid of DC and AC. Hence a DC microgrid is the best option in RES, power converters, and modern loads all require DC electricity to operate.

Furthermore, the structure’s simplicity, great energy efficiency, isolated operation mode, and consistent power delivery to remote locations make it a good choice. For regulated DC bus voltage and steady operation, multiple nonlinear controller control techniques are employed. An MG has been built using terminal sliding mode control (SMC), but the system is susceptible to external disturbances and has inherited chattering effects. The use of double integral sliding mode controllers for energy harvesting and DC microgrid management integrating RES and a hybrid ESS has been proposed in [9]. A new intelligent control technology known as the Brain Emotional Learning-Based Intelligent Controller (BELBIC) was employed in [10]. The control and energy management of the hybrid system was utilizing the proposed controller.

Many control algorithms for wind/PV control systems have been proposed in the literature. To control MG in the past, PI/PID linear control, SMC, and artificial intelligence-based control were all used. Nonetheless, in the last decade, intelligent control of nonlinear systems has gotten a lot of attention [11]. As a result, common controllers such as neural networks, and fuzzy and neuro-fuzzy controllers have been researched. Parameter linearization, high learning capabilities, built-in universal approximation, and model-free operation are only a few of their advantages. As a result, it has an excessive number of uses in non-linear control, adaptive control, robust control, robotics, and decision making [12-13]. In 1965, Zadeh introduced fuzzy logic for use in cellular robotics, and since then, numerous sorts of studies have adopted this logic to various model-based control systems. It provides a framework for understanding the complete model’s uncertainties and opacity using human reasoning based on membership functions and linguistic variables. The application of the fuzzy logic controller (FLC) to power system operation and control has gotten increased attention in recent years [14]. This paper discusses the controller framework for regulating voltage regulation in a microgrid with RES and an energy storage system. The self-tuning fuzzy proportional-integral-derivative (SFPID) controller was proposed in [15] which gives better performance in terms of

overshoot, rising time, and settling time. As a result, a RES-based Fuzzy controller for loads input into the microgrid has been presented. The objective is to maximize the usage of RESs as much as feasible, maintain voltage regulation, and ensure that the important load is fed continuously.

## 2. Literature Survey

When planning and evaluating the performance of an off-grid hybrid system, the dependability of the system, the cost of power generation, and the operating environmental impact are the most important considerations. Tarife *et al* [16] used multi-objective particle swarm optimization (MOPSO) and a proposed multi-case power management strategy to present an integrated method for optimal sizing and operation of a proposed system for rural agricultural communities composed of hydropower, PV, diesel generator, and a battery energy storage system (BESS). Punna *et al* [17] proposed a multi-input bidirectional DC-DC power converter (MIPC) with an upgraded converter for a hybrid (ESS). The charge and discharge rates of batteries used for energy storage are low, putting the battery under current stress and decreasing its life. Therefore, Supercapacitors (SCs) can react quickly to abrupt variations and alleviate this problem due to their enhanced power density. The suggested model predictive control (MPC) provided improved DC grid voltage restoration to step changes in PV generation and load demand. The MPC approach reduces current stresses, extends battery life, and improves overall system performance while also offering faster DC grid voltage control.

Doshi *et al* [18] created an integrated RES model based on simulation. The system functions as a DC microgrid, including renewable generators such as solar and wind, lithium-ion battery storage, and inductive loads. The solar PV generator is connected to the DC microgrid via a SEPIC converter, while the wind generator is connected via an AC/DC converter. Depending on the availability of RES, power flows from the DC bus to the loads and between the load and the batteries. Nevertheless, rural hybrid systems' optimal planning is a difficult and time-consuming undertaking, especially when numerous options and sustainability factors are taken into account. Ullah *et al* [19] proposed an integrated decision-making scheme for the best planning of a RES supply system that includes solar, wind, hydro, and biomass sources. A designed analysis of twelve on/off-grid electrification options is performed on an hourly basis. The suggested model incorporates a fuzzy analytic hierarchy process, and multi-objective optimization using the ratio analysis approach for order of preference based on resemblance to an ideal solution.

Suman *et al* [20] used a combination of solar/wind/bio-generator energy generation devices, as well as diesel generation and the battery. For optimization, a hybrid PSO-Grey Wolf Optimiser (GWO) is used. The results are compared to those obtained using other previously published methods, and the efficacy of the developed approach is determined. The financial benefits of combining energy efficiency practices and hybrid PV-biomass distributed generating systems to create standalone rural homes in Morocco are evaluated by Allouhi *et al* [21]. In the Fez region, this integrated analysis technique improves the economic and conservation sustainability of rural housing units. It employs optimized selection processes to identify both energy efficient and RES technologies that are widely available in the region to reduce housing unit costs and energy use. Chaudhary *et al* [22] present a non-isolated integrated multiple output synchronous buck converter to meet the auxiliary power supply requirements of E-Mobility. In comparison to typical separate buck converters and conventional synchronous buck converters, the converter delivers independently controlled numerous outputs with a lower switch count. By altering the duty ratio of the

linked switch, each converter output may be controlled independently, effectively eliminating the problem of effective cross-regulation.

A modern metaheuristic strategy of sparrow search algorithm (SSA) was used by Fathy *et al* [23] to manage the operation of MG an optimal-wise. PV, wind, fuel cell, micro-turbine, BSS, and grid are among the MGs examined. Due to the huge number of equipment and diverse control loops in the Hybrid RES, an efficient control technique to coordinate the ESS with other equipment within HRES is required for an effective contribution of ESS. To fill this void, a PI-based control synthesis method for adjusting PI controllers in Nezhad *et al* [24] is provided. PI controllers for various types of ESS are constructed using the suggested method, which takes into account root-locus trajectory, dominant pole damping coefficient, and equipment coordination. Elkasem *et al* [25] developed an intelligent control technology to improve the frequency dynamic performance of interconnected multi-source power systems containing thermal, hydro, and gas power plants, as well as the high penetration of wind energy. To circumvent the PID constraints during abnormal conditions, the suggested control technique uses an integration of fuzzy logic control and a PID controller. Furthermore, to avoid the shortcomings of conventional and heuristic optimization strategies, a novel adopted optimization technique called the Arithmetic optimization algorithm was proposed to fine-tune the proposed fuzzy-PID controller.

## 3. Research Problem Definition and Motivation

Renewable energy sources including solar photovoltaic (PV), solar thermal, geothermal, wind, biomass and hydro are considered promising alternatives for clean heat and power generation. These sources can provide sustainable energy to all populations irrespective of their geographical location and financial status. Due to the decentralized nature of these sources, small Hybrid Power Systems (HPS) can be deployed even in remote locations. The present degradation of the global environment has empowered authorities in various countries to adopt energy strategies that promote clean energy generation alternatives and foster energy efficiency programs. Worldwide, the building sector accounts for approximately 36% of the total final energy use. Thus, enhancing its energy efficiency is crucial to achieving the desired decarburization targets. The present work is the design optimization and assessment of hybrid RES solar/wind/battery/biomass in the context of the energy sector. The model addresses the feasibility investigation of both on/off-grid rural electrification scenarios. In each scenario, hybrid configurations are modelled, optimized, analyzed, and compared. Micro-grids are becoming increasingly popular due to their flexible design, resilient operation and providing reliability, robustness and power quality in the electric power supply network. They can switch between grid-connected and islanded modes of operation which offers a high degree of security. The management of power in such a grid becomes important for voltage and frequency control. Different voltage and frequency control strategies have been successfully implemented within AC and DC grids, but the control of hybrid microgrids requires further attention with a focus on ILC. This motivates the research to propose an energy-efficient power management strategy with the designed hybrid DC/AC microgrid with four renewable energy resources.

## 4. Research Proposed Methodology

The objective of smart power systems is to combine all renewable energy sources to increase the electricity supply of clean energy sources. Microgrids provide a new infrastructure for more efficient, resilient and cost-effective power systems. The proposed methodology seeks a model for

minimizing the Energy Cost (EC) and enhancing the power supply for rural areas by designing and analyzing four different hybrid system configurations based on integrating a biomass system with a photovoltaic (PV), wind turbine (WT) and battery system. This research proposes the power management of hybrid DC/AC MG with the efficient use of RERs. Figure 1 illustrates the block diagram of the proposed work.

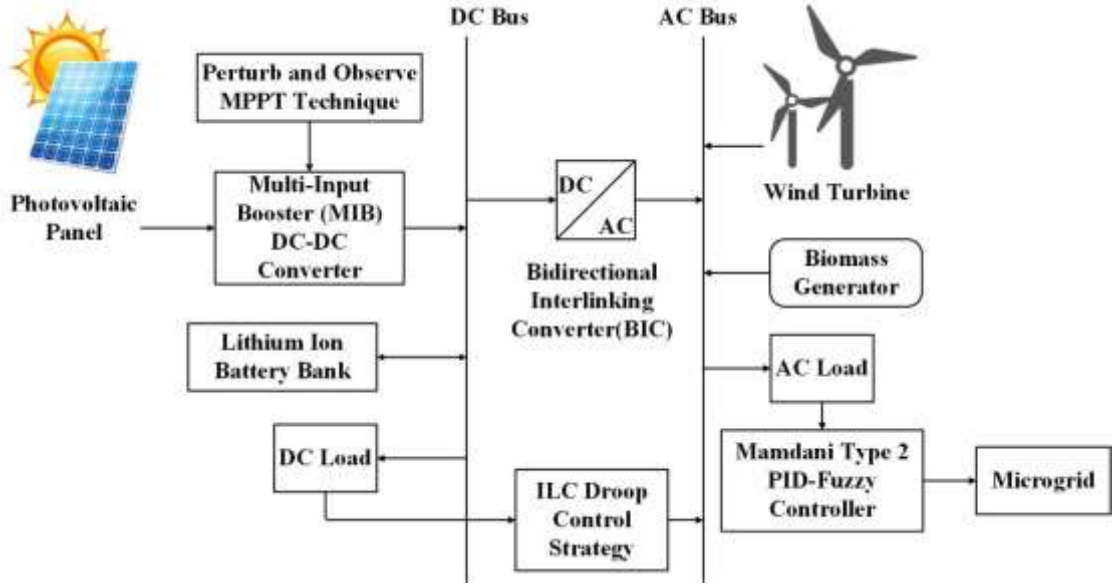


**Figure 1:** Block Diagram of the Proposed Work

The research proposed the energy-efficient hybrid RES (solar, wind, biomass and battery) for power management in a microgrid. Power electronic converters are utilized to connect these sources to the supply network through a common grid bus. Consequently, the study employs the DC/AC microgrid grids tied by an Interlinking Converter (ILC). Mamdani type 2 PID-fuzzy controller into the high-type control system, is proposed to overcome load fluctuations of the microgrid. This attains high performance and desirable responses for different scenarios of change in load. The proposed system is implemented in MATLAB/Simulink to verify the effectiveness of this control strategy. The procedure for the operating strategy can be summarized in the following steps. Case study site selection was guided by the availability of solar energy and biomass resources which can be used in building the hybrid off-grid system.

### 4.1 Modelling of AC/DC Microgrid

Microgrids have become an attractive option for distributed generation (DG) with the increase in Renewable Energy Sources (RES) and storage systems. Microgrids (MGs) are designed with the help of effective power extracted from renewable sources such as solar, wind, battery, and biomass. Furthermore, particularly when paired with renewable generators, batteries help provide reliable and cheaper electricity in isolated grids and off-grid communities. Lithium-ion batteries were chosen for this study due to their high energy density, long life cycle, and high efficiency.

#### 4.1.1 Modelling of the Solar PV system

Weibull PDF is used to characterise the stochastic behaviour of the solar irradiance as it provided a good fit for the irradiance data of the chosen site compared to beta, gamma, lognormal and generalized extreme value distribution (GEV) PDFs. At any timeframe ‘ $t$ ’, the Weibull distribution for the solar irradiance $s\left(w/m^2\right)$ is given

by Equation (1), and the shape parameter $k^t$ and the scale factor $(c^t)$ are calculated at the time frame '$t$' using the maximum likelihood estimation (MLE) method.

To analyse the solar PV output power, the continuous PDF is divided into different states for a particular time frame. Solar irradiance will be within limits in each state, the probabilities of all possible states for that particular hour are obtained, and these probabilities are used to obtain power generation in the time segment. The average power output of the solar PV array for a particular time frame't' or hour is given by

$$P_{pv}(t)=\sum_{st=1}^{N_s} P_{pv}\times P_s\left(s_{st}^t\right) \tag{2}$$

For a given state, during any particular time frame or any particular hour, the solar irradiance probability is given by

$$P_s\left(s_{st}^t\right)=\begin{cases}\int_0^{\left(s_{st}^t+s_{st+1}^t\right)/2} f(s_t)ds & for\ st=1\\ \int_{\left(s_{st-1}^t+s_{st}^t\right)/2}^{\left(s_{st}^t+s_{st+1}^t\right)/2} f(s_t)ds & for\ st=2\ldots(N_s-1)\\ \int_{\left(s_{st-1}^t+s_{st}^t\right)/2}^{\infty} f(s_t)ds & for\ st=N_s\end{cases} \tag{3}$$

If the power generated by the PV array with the average solar irradiance (i.e. if a state represents solar irradiance $\left(w/m^2\right)$ is lying between 0 to 100, then the average ( $s_{st}^t$ will be 50 $\left(w/m^2\right)$) for $st-th$ the state is calculated as

$$P_{pv}=N_{pv}\cdot f_{pv}\cdot\eta_{mppt}\cdot ff\cdot I_{sc}(st)\cdot V_{oc}(st)$$

$$f(s_t)=\frac{k^t}{c^t}\cdot\left(\frac{s^t}{c^t}\right)^{k-1}\cdot\exp\left(-\left(\frac{s^t}{c^t}\right)^{k-1}\right) \quad for\ c^t>1;k^t>0 \tag{1}$$

$$ff=(V_{oc}\cdot I_{sc})/(V_{stc}\cdot I_{stc}) \tag{4}$$

### 4.1.2 Modelling of the Wind Energy System

Weibull PDF is suited to express the wind speed stochastic behaviour, as it provides a good fit for the wind speed distribution at the chosen site. Weibull PDF for the wind speed $v(m/s)$ for any time frame $t$ can be expressed as

$$f(v_t)=\frac{k^t}{c^t}\cdot\left(\frac{v^t}{c^t}\right)^{k-1}\cdot\exp\left(-\left(\frac{v^t}{c^t}\right)^{k-1}\right) \quad for\ c^t>1;k^t>0 \tag{5}$$

The average output power of the wind turbine (WT) for a particular time frame $t$ or a particular hour is given by

$$P_{wt}(t)=\sum_{st=1}^{N_v} Pwt_{st}\times P_v\left(v_{st}^t\right) \tag{6}$$

The power generation of the WT depends on the velocity of the wind at that particular time. Therefore, the power generated by WT at the average wind speed $v_{st}^t$ for any state $st$ is determined as

$$Pwt_{st}=\begin{cases}P_{rw}\cdot N_w\cdot\left(\frac{v_{st}^t-v_{ci}}{v_r-v_{ci}}\right) & for\ v_{ci}<v_{st}^t<v_r\\ P_{rw}\cdot N_w & for\ v_r<v_{st}^t<v_{co}\\ 0 & else\end{cases} \tag{7}$$

### 4.1.3 Modelling of Biomass Gasifier

Thermochemical conversion technology is used to convert biomass into clean and cool gas by partial combustion under a restricted air supply. This produced gas is used as an input for the fuel engine to generate electricity. In this study, a 10 kW rated biomass gasifier is considered, which is operated for 12 h per day during the peak load. The total annual biomass energy generated is given by Equation (8):

$$E_b = N_b \times P_b \times t_w \tag{8}$$

The maximum rating of the gasifier depends on the total available biomass in a year, the calorific value of biomass and the efficiency of the biomass gasifier, which is given by

$$p_b^{\max} = \frac{total * 1000 * CV_{bm} \times \eta_b}{365 * 860 * t_{bio}} \tag{9}$$

### 4.1.4 Modelling of Battery

Lead-acid batteries are used in this study because of their short response time, low self-discharge rate (3%–20%), high cycle efficiency (70%–85%), and low capital cost. BESS is chosen to supply the peak load demand for at least 30 min. To operate BESS reliably and efficiently, a complete study of battery requirements while charging and discharging, energy loss and efficiency is required. If the total energy generated from the PV, biomass, and wind is more than the energy demand, then the battery bank will charge, and whenever there is an energy deficit to meet the load, the energy stored in the battery will supply the deficit energy to the load. The state of charge (SOC; which represents the amount of energy stored in the battery) controls the performance of the HRES.

**State of Charge**

The original SOC of battery in charging mode is given by

$$SOC_{org}(t+1) = SOC(t) + \frac{I_{bat}(t) \cdot \Delta t}{C_{bat}} \tag{10}$$

But due to battery self-discharging rate $(sdr)$; which depends on the health state of the battery and accumulated charge) and battery charge efficiency factor $(\eta_c)$ the actual SOC of the battery is less than $SOC_{org}$ and is described as

$$SOC(t+1) = SOC(t) \cdot (1 - sdr) + \frac{I_{bat}(t) \cdot \Delta t \cdot \eta_c(t)}{C_{bat}} \tag{11}$$

The charge efficiency factor is described as

$$\eta_c(t) = 1 - \exp\left[\frac{a.(SOC(t) - 1)}{(I_{bat}(t)/I_{10} + b)}\right] \tag{12}$$

Where working condition parameters of the battery $(a, b, I_{10})$ are considered as 20.73, 0.55, and 10, respectively. The charging current $I_{bat}(t)$ at any time $t$ can be derived for HRES (which gives the amount of excess power generated by RES after supplying the load) and is given by

$$I_{bat}(t) = \frac{P_{pv}(t) + P_{wt}(t) \cdot \eta_{re} + N_b \cdot P_b(t) \cdot \eta_{re} - (P_l(t) \cdot \eta_{in})}{Nb_{st} \cdot Nb_{se} \cdot V_{bat}} \tag{13}$$

To convert AC power generated by biomass and wind into constant voltage DC power, a rectifier is used. BESS is operated subjected to the constraints as follows:

$$SOC_{\min} \le SOC(t) \le SOC_{\max} \tag{14}$$

And

$$I_{bat,\max}(t) = \max\{0, \min[I_{\max}, C_{bat} \cdot (c \cdot (SOC_{\max} - SOC(t)) + (SOC(t) - SOC_{\min}) \cdot (1 - c))/\Delta t]\}$$

Where $SOC_{\max}$ is the SOC maximum value, which is 1; $SOC_{\min}$ is the SOC minimum value, which is chosen as 30%. The maximum achievable current rate of the battery $I_{bat,\max}$ at any given point in time depends on the state of the battery. Here, Imax is considered as 20% of its nominal capacity for the long life of the battery, $c$ is considered to be 0 while discharging, and is chosen as 1 while charging.

**Grid-Tied Operation**

Grid-connected mode is further classified into two types based on the contract. i) Non-dispatched power: In this mode, DGs operate in MPP, and excess power

generated after meeting local loads is fed to the grid ii) Dispatched power mode: In this mode, DC bus voltage is regulated in two ways a) Interlinking converter (ILC) is controlled to regulate DC link voltage, and DG units on AC bus and DC bus are harmonized for supplying dispatched power with power balancing. DC-DC converter runs PV and wind generators at maximum power point in normal mode or power flow control mode, charging the battery from the grid and discharging when power generated by PV and wind is less than demanded power from the grid. DGs connected to the AC bus and interlinking converter are operating in power flow control mode, and DGs connected to the DC bus are responsible for DC link voltage regulation. Power-driven into to grid can be controlled by changing the phase angle and magnitude of the fundamental voltage of the inverter for the grid. The existence of both AC and DC microgrids has led to a new concept of hybrid AC/DC microgrids which consists of both AC and DC grids tied by an Interlinking Converter (ILC). It comprises a DC grid and AC grid interlinked by a bidirectional DC/AC converter. Such a hybrid AC/DC microgrid has the advantages of both AC and DC with increased efficiency and less cost. The DC comprises a PV panel system and a battery bank storage system. The DC loads are connected to the DC via the DC bus. The AC comprises the wind turbine (WT) system and Biomass.

### 4.2 Bidirectional DC/AC Converter

Converters play an important role in the synchronization process. The bidirectional DC/AC converter is an online converter which is common between the DC bus and the AC bus. It allows the bidirectional flow of power between DC bus and AC bus. It can work both as an inverter and as a rectifier. When there is a power deficit in the DC MG, the converter works as a rectifier and power are supplied from the AC side to the DC MG, thereby preventing the isolation of the loads connected to the DC bus. The voltage source control technique is used which has precise control over the magnitude, phase, and frequency of the voltage. The bypass diodes which are antiparallel to the switches help in the circulation of reactive power and the flow of active power in both directions. The sinusoidal pulse width modulation technique is used as the switching scheme.

An important feature of grid-connected DC microgrids or DC distribution systems is the ability to inject or suck power from the grid based on the generation and loading conditions. To do that, a controlled AC-DC/DC-AC converter that allows bi-directional power flow has been designed. This controlled converter is responsible for controlling the amount of power flowing between the AC and the DC grids. Power flow from the AC to the DC grid is very important to cover any deficiency in the demand in the DC grid due to normal or pulse loading. Moreover, Power flow from the DC to AC grid is needed when there is an excess in power from renewable energy sources on the DC bus. The current on the DC side is assumed positive if flowing from the Ac grid to the DC system and vice versa. Hence, if $i_{dc}^{ref}$ is set to a positive value, the bi-directional AC-DC/DC-AC converter will autonomously operate in the rectifier mode and the modulating signals will be lagging the grid voltage. However, if it is set to a negative value the modulating signals will be leading and the DC network will inject current to the AC grid. In both modes of operation, the vector decoupling technique used allows unity power factor operation by setting $i_d^{ref}$, which is responsible for the reactive power, to zero. The fully controlled bi-directional converter is operated at an 8 kHz switching frequency and sampling time of 0.3 ms, which allows the controller to detect and respond quickly to different load demands at either the AC or DC sides. The converter is designed to operate at a low THD and unity power factor. A 24 mH inductor with 0.9-ohm losses is connected between the AC grid and the converter to filter

harmonics associated with the fundamental current waveform.

### 4.3 DC-DC Converter

Only certain solar panels mostly in the sector are 12 or 24V (2 to 5A), however, the load requirements involve higher voltages, requiring the use of a boost converter. DC-DC converters are being used as a power converter in between load and source to enforce and increase the PV depending on the voltage output signal. Further, the work is focused to build a new boost converter of Multi-Input Booster (MIB) converter for high gain system and its equivalent system with a perturb and observing algorithm-based maximum power point tracking control mechanism to extract maximum power from the solar PV system. This Multi-Input DC-DC converter improves DC side load sharing and DC bus voltage regulation of ILC along with battery SOC control of individual DC-DC converters in the DC microgrid (DCMG). DC link voltage of ILC is regulated usually by DC side control in load sharing among sources in the DC microgrid. AC microgrids are based on the ILC droop control coefficients of sources on either side and transfer power from DC microgrid to AC microgrid and vice-versa. Additionally, the ILC control prevents any negative sequence currents from entering the AC source.

#### 4.3.1 Multi-Input Booster (MIB) DC-DC Converters

Only certain solar panels mostly in the sector are 12 or 24V (2 to 5 A), however, the load requirements involve higher voltages, requiring the use of a boost converter. Multi-Input Booster (MIB) DC-DC converters are being used as a power converter in between load and source to enforce and increase the PV depending on the voltage output signal. The multi-input converter is a circuit structure that integrates different input voltage sources with different voltage levels and supplies an output dc load. According to the principles of circuits and systems, the syncretization of dc-dc converters depends on whether it consists of a pulsating current source or pulsating voltage source. In the case of pulsating current sources such as boost converters, these modules need to be connected in parallel to supply the load. The proposed multi-input converter is depicted in Figure 2. The power management unit will control all the systems to keep the DC bus at constant high voltage and charge and discharge the batteries. It consists n pulsating current sources derived from the boost converter, an inductor$L_0$, a capacitor $C_1$ and a voltage sink that consists of a capacitor $C_0$ and the load. Each of the pulsating current sources includes an inductor$(L_1 - L_2)$, a power switch $(S_1 - S_2)$ and a diode $(D_1 - D_2)$and are connected to different voltage sources with different voltage levels namely$V_1 - V_2$. Moreover, the capacitor $C_1$ and the inductor $L_3$ are to ensure the continuity of the output current regardless of the switching scheme.

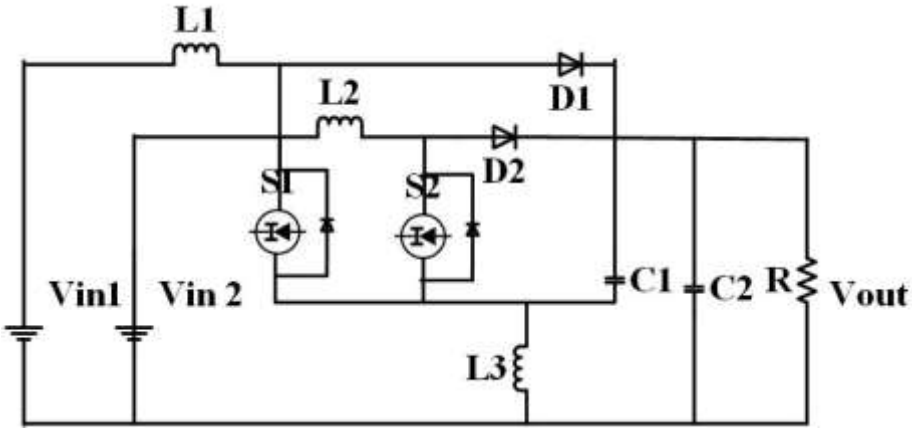


**Figure 2:** Multi-Input Boost Converter

Every small ensemble of wind turbine (600 watts) and PV (400 watts) is mounted on electricity poles. All these electricity poles ensembles are connected in parallel to each other, for simulation results around 40 units of this collection are selected and a summation of their output voltage will charge the batteries. The power applied to boost the converter will equal the summation of powers gained from all units. To achieve maximum power point in wind systems, the rotational speed of the turbine rotor shall be immediately adjusted with wind velocity. In the MIC, the perturb-and-observe method is employed to draw maximum power from wind turbine and PV arrays since it is easy to carry out. Maximum Power Point Tracking often referred to as MPPT, is an electronic system that operates the Photovoltaic (PV) modules in a way that allows the modules to generate all the power they are capable of. It is used to automatically find the maximum power point voltage (VMPP) or maximum power point current (IMPP) at which a PV array should function to produce the maximum output power under a given temperature and irradiance. The Perturb & Observe algorithm is one of the most widely used methods for MPPT control. Few measurements and a feedback loop are needed. The block diagram of the P&O method is shown in the figure. Initially, the solar panel voltage is intentionally perturbed (increased or decreased) by a small increment value, then the resultant power is compared to the power which is obtained before the disturbance occurs. Particularly, if the power panel is increased due to the disturbance, the disturbance which follows the previous one will be made in the same direction. Further, if the power decreases, the new perturbation is made in the opposite direction.

### 4.4 ILC Droop Control Coefficient

To address these shortcomings, this paper proposes a novel, generalized droop scheme of ILC for autonomous power-sharing and control of a hybrid microgrid. A standalone hybrid microgrid is considered where the control of active power is more complex as compared to the grid-connected mode. The ac microgrid operates on frequency droop while voltage droop is used in the dc microgrid. A 3-dimensional plane is proposed for ILC control where the axis corresponds to dc voltage, ac frequency and converter power. The converter utilizes frequency droop at the ac terminal and voltage droop at the dc terminal so any change in dc voltage or ac frequency results in active power flow from an underloaded to the overloaded grid. The three quantities, namely active power, ac frequency and dc voltage, are introduced in the outer control loop of the converter along with three scaling factors which define the converter frequency and voltage droop.

To enable autonomous power-sharing between ac and dc grids, dc voltage droop and ac frequency droop are implemented in the outer control loop of the converter. Any load change in the ac grid will result in frequency variation and the power flow through the converter will change according to the frequency droop. Similarly, any dc load change will result in voltage variation which will change the converter power according to the dc voltage droop. Taking into account the fact that the converter does not generate any power and neglects converter losses, the following relation can be established.

$$k_1\Delta V_{dc} + k_2\Delta P_c - k_3\Delta f = 0 \quad (15)$$

Further expansion of this expression yields:

$$k_1\Delta V_{dc} + k_2 P_c - k_3 f - \left(k_1 V_{dc,ref} + k_2 P_{c,ref} - k_3 f_{ref}\right) \quad (16)$$

This is the generalized droop control which combines dc voltage and ac frequency. The maximum power flow through the tie line between ac and dc grids is represented as $P_{c,ref}$. The droop coefficients define the power flow through the converter. Equation (16) is a plane $ax + by + cz + d = 0$ drawn on the axis. If $k_1$ is set to zero, the converter operates in frequency droop and the droop coefficient is set by the ratio of $k_2$ and $k_3$ as shown in (17). This droop line is drawn on the plane on $f - P_c$ axis. In this case, no change in active power is observed due to load change in the dc grid and converter power is only dependent on ac grid frequency.

$$\frac{\Delta f}{\Delta P_c} = \frac{k_2}{k_3} \quad (17)$$

A voltage-frequency droop can be established by setting $k_2$ zero. In this case, the droop coefficient is given by

$$\frac{\Delta V_{dc}}{\Delta f} = \frac{k_3}{k_1} \quad (18)$$

This droop coefficient is the slope of the line drawn on $V_{dc} - f$ axis on the plane. Any change in dc voltage is translated into a change in frequency of ac grid but there is no control on the active power flowing through the converter. Any change in ac grid load will vary the power generated by the ac grid and the power flow through the converter according to the following relation:

$$\Delta P_L = \Delta P_{g,ac} - \Delta P_c \quad (19)$$

The load change in the ac sub-grid will cause frequency change. According to frequency droop, the change in ac power generation due to a change in frequency is given by:

$$\Delta P_{g,ac} = \frac{2\pi}{m}\Delta f \quad (20)$$

From the control scheme of the converter, the total change in active power $\Delta P_c$ from ac grid to dc grid is given by:

$$\Delta P_c = \frac{k_3\Delta f - k_1\Delta V_{dc}}{k_2} \quad (21)$$

Substituting (20) and (21) in (19) gives us:

$$\Delta P_L = \frac{2\pi}{m}\Delta f - \frac{k_3\Delta f - k_1\Delta V_{dc}}{k_2} \quad (22)$$

This equation describes the impact of the ac load change on ac frequency and dc voltage in a hybrid microgrid. The change in power consumed by dc load can then be expressed as:

$$\Delta P_L = \frac{\Delta V_{dc}}{n} + \frac{k_3\Delta f - k_1\Delta V_{dc}}{k_2} \quad (23)$$

This relation can be used to determine its effect on frequency and dc voltage. Different voltage and frequency control strategies have been successfully implemented within AC and DC grids, but the control of hybrid microgrids requires further attention with a focus on ILC.

### 4.5 Controller System

The voltage and frequency of MGs are strongly impressionable from the active and reactive load fluctuations. A change in load leads to an imbalance between generation and consumption. The output voltage and frequency of the DGs are primarily controlled by the droop characteristics. But, in case of severe changes in load, the DGs may be failed and the Microgrid is collapsed. Subsequently, the research proposed the intelligent Mamdani type 2 PID-fuzzy controller into the high-type control system, which exhibits high performance and desirable response for different scenarios of change in load.

### 4.5.1 Mamdani Type 2 PID-Fuzzy Controller

A fuzzy action is also occurred between the grades of type-II membership functions due to which it can enhance the fuzziness and simultaneously imprecise data and is controlled in a precise manner. Figure 3 depicts the entire process incurred with the type-II fuzzy system. Mamdani 2FLC. This explained that there are five interconnected blocks in this figure, i.e., fuzzifier, rules, inference, type reducer and defuzzifier. A mapping exists between crisp inputs to crisp outputs of the IT2FLS and is expressed as $Y = f(x)$. The fuzzifier converts crisp inputs X to an interval type-2 fuzzy set. The general configuration for both T1FLS and IT2FLS is the same, but the only difference is that the antecedents and consequents of IT2FLS are represented as type-2 fuzzy sets.

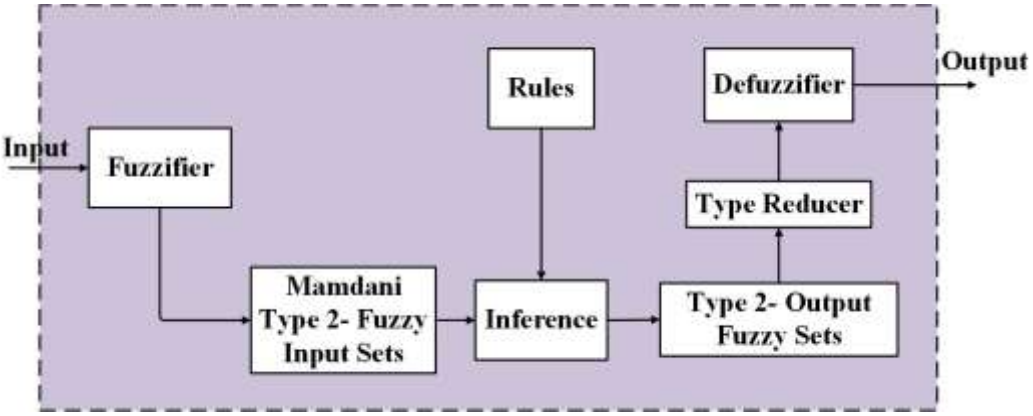


**Figure 3:** Block Diagram of Type II Fuzzy Controller

Rules are combined through an inference engine. It produces output type-2 fuzzy sets from input type-2 fuzzy sets. The type reducer reduces the type-2 fuzzy sets into a type-1 fuzzy set output. Through a defuzzifier, it is converted into crisp output. Crips output can be applied to a particular plant which has to be controlled.

### 4.5.2 Design of Type-2 Fuzzy PID Controller

To describe details of the type-II fuzzy controller along with fuzzification and fuzzification it goes through different steps. In general, the fuzzy control rules of the discrete Mamdani controller [23], which has three inputs e1(k), e2(k), e3(k) and one output u(k), will be written as

$$R^{\theta}: \; if \; e_1(k) \; is \; E_1^{\theta}, \; e_2(k) \; is \; E_2^{\theta}, \; e_3(k) \; is \; E_3^{\theta} \quad (24)$$

$$u(k) = U^{\theta}$$

Using the ‘and’ function, the antecedent part of all rules is created. In this simulation, Mamdani fuzzy inference system has been applied. T1 Fuzzy sets showed limitations in the ability to model and minimize the effect of uncertainties. That is because the T1 fuzzy set is certain in the meaning that its MF degrees are crisp

values. On the other hand, the type-2 fuzzy sets were described by membership functions that are themselves fuzzy which attracted more attention. Since the scope of fuzzy control is very wide, various controller structures are possible, differing in the number of inputs and outputs, their fuzzy sets, membership functions, fuzzification method, a form of control rules, type of output mechanism and method of defuzzification. A Mamdani type of fuzzy engine is perceived, and the FLC output is calculated by using the defuzzification method of the centre of gravity. The parameters K1 and K2 are scaling factors, and the gains of the PID are indicated with KP, KI, and KD, and N represents the filter coefficient. Four types of inference schemes (including Mamdani's) have been investigated by Ying, but a uniform equation for the composed fuzzy output was derived.

## 5. Experimentation and Results Discussion

To obtain the above response the two-area transfer function model of interconnected MG system is developed in Simulink environment and necessary programmes are written in .m file of MATLAB2021 software through 4GB ram, Intel Core i5 @ 3.5GHz processor-based system. The ac and dc sub-grids are modelled. For load frequency control, the system uncertainties are affected individually and finally in combined form to trace out different dynamic responses. A computer model of the proposed PV-fed dc-bus charging station system and the corresponding control schemes are built-in MATLAB/Simulink. The nominal frequency of the ac grid is 50 Hz and the voltage of the dc microgrid is 800 V. The converter reference power is set at 10 kW which indicates the maximum power that can be delivered to the dc microgrid. The effect of coupling on the defined droop coefficients is also discussed in both scenarios with different load changes within the hybrid microgrid.

**Table 1:** System Configuration

| | |
|---|---|
| MATLAB/Simulink | R2021a |
| Operating System | Windows 10 Home |
| Memory Capacity | DDR3 |
| Processor | Core i5 @ 3.5GHz |

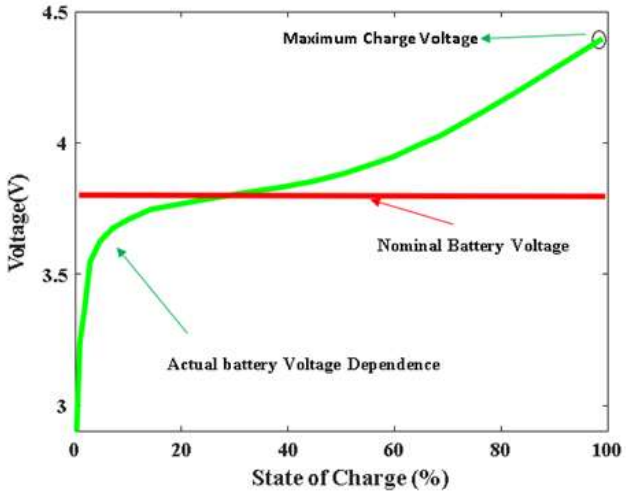


**Figure 4:** Typical Discharge Curve of Lithium Ion Cell

Figure 4 illustrates the maximum discharge voltage with the actual battery voltage dependence. Lithium-ion cells also require much tighter voltage tolerance on detecting full charge and once fully charged they do not allow or require to be trickle or float charged. It is particularly important to be able to detect the full charge state accurately because lithium-ion batteries do not tolerate overcharging. They over-heat and this reduces their life but in extreme circumstances, it can lead to them catching fire or even exploding. Most consumer-orientated lithium-ion batteries charge to a voltage of 4.5 volts per cell and this has a tolerance of around ± 50 mV per cell.

**Performance Ratio (PR)**

It is the actual amount of energy produced by a PV system to the energy produced by the same system when operating continuously at standard test conditions (STC) and the same global irradiation, therefore,

$$P_R = \frac{Generated\ \ Energy\ \ from\ the\ PV\ \ System}{Total\ \ Incidence\ Global\ Radiation\ on\ PV\ \ Array(kwh)\times \eta_{stc}} \quad (25)$$

Where, $\eta_{stc}$ is PV panel efficiency at standard test conditions. $P_R$ is independent of system size and is typically evaluated on a monthly or yearly basis by considering system total losses. Equation (4) shows that PR does not change a lot with the type of the PV system and depends basically on the constant STC values. In large-scale commercial systems, PR can be used to investigate the occurrences of component failures by calculating them for smaller intervals, such as weekly or daily. The average value of the performance ratio found in the literature is within the range of 0.6 to 0.9.

**Performance Index (PI)**

The performance of the power generator when considering thermal losses due to PV panel overheating and the inverter operation losses. It allows comparing the PV system under different climatic and installation conditions. The value of PI was found in the range of 84% - 85% and it can be calculated by.

$$PI = \frac{Generated\ \ Energy\ \ from\ the\ PV\ \ System\ in(kwh)}{Total\ \ Incidence\ Global\ Radiation\ on\ PV\ \ Array(kwh)\times \eta_{pv}} \quad (26)$$

Where, $\eta_{pv}$ is PV panel efficiency at actual surface temperature,

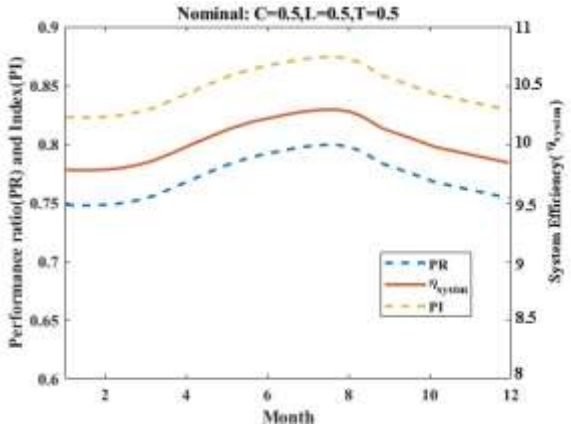


**Figure 5:** Performance Ratio and Index for 12 Months

Figures 5 show that the module produced a high monthly efficiency and performance ratio during the days with low ambient temperature than on the other days.

These two indicators show that the maximum system performance occurs in winter while the minimum system performance occurs in summer. This trend in system performance is because these indicators use input irradiation as a reference for comparison.

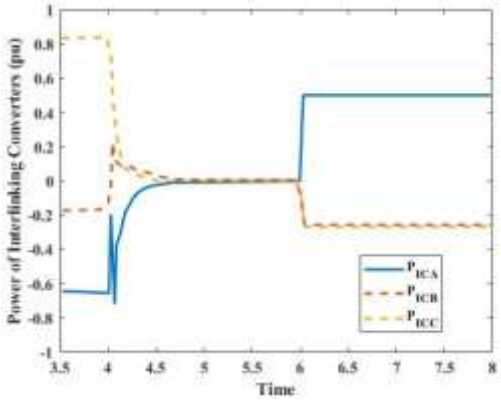


**Figure 6:** Power of Interlinking Converters

Figure 6 illustrates the power of the interlinking converter. This validates the effectiveness of the proposed method, we are assuming that the DC-AC faults, as an example, at t = 3s. The dynamics of the power outputs of the power units, the common DC bus voltage, the DC voltages, the AC frequency, the power outputs of the balance units in AC/DC microgrids and the power outputs of the ICs are presented, respectively.

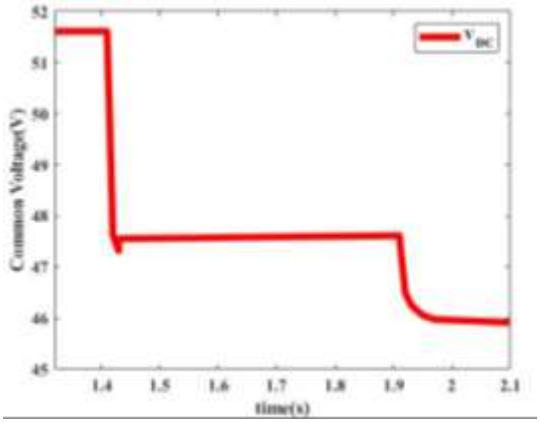


**Figure 7:** Common Voltage of Bus

Figure 7 gives the simulation results of the hybrid DC/AC microgrid voltage with the dc-bus voltage. Due to the battery current, the dc-link voltage drops slightly, but it remains between 12% and −20% of the rated voltage (540 V).

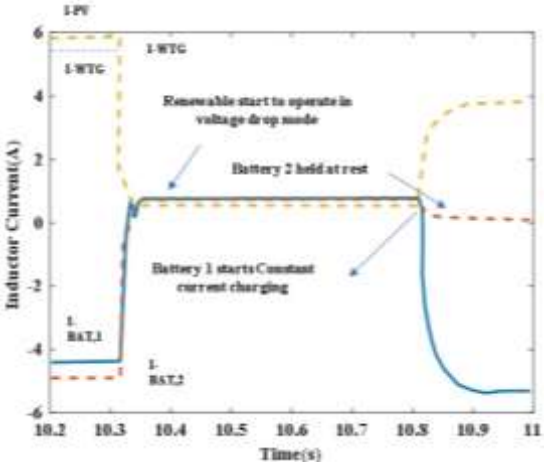


**Figure 8:** Inductor Current

Figure 8 illustrates the graph of the inductance current. When a battery is connected to a series resistor and inductor, the inductor resists the change in current and the current therefore builds up slowly. Establishing a current in an inductor stores energy in the magnetic field formed by the coils of the inductor. It can be seen that the current is zero through the inductor at the onset and gradually increases to the maximum value as it stores the energy magnetically. The yellow line indicates the voltage across the inductor for the same. This can witness it to be maximum at the switch ON instant, which gradually dies down to the lowest value during the inductor energy storage.

**Voltage Gain**

The voltage gain of boost converter is expressed as:

$$M_b = \frac{1}{1-D} \tag{27}$$

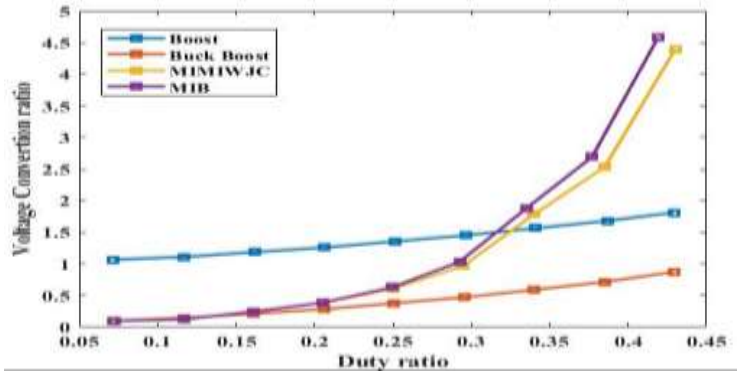


**Figure 9:** Voltage Gain Comparison

The comparison between the voltage gain and duty cycle of the proposed converter and other converters is plotted in Figure 9. One can observe that the voltage gain of the proposed converter is higher than that of a conventional boost converter and twice as much as that of a quadratic converter under the same duty cycle. The voltage gains of the converter in [27] where a coupling inductor exists are higher than the proposed converter at the duty cycle under 0.55. However, the proposed converter provides the highest voltage gain among these converters when the duty cycle is larger than 0.55

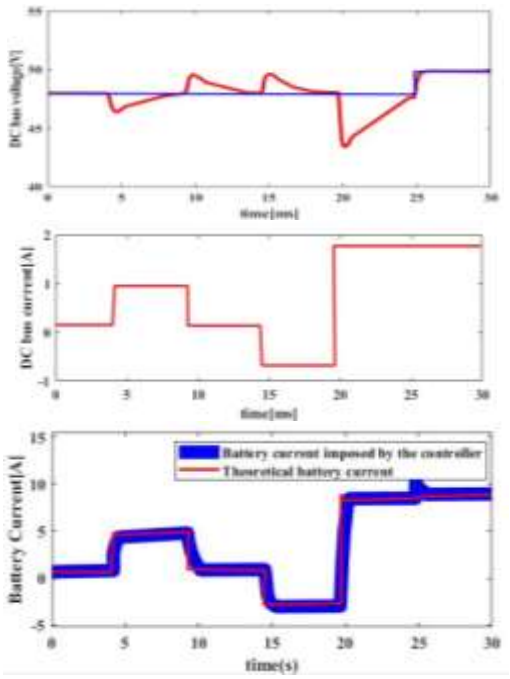


**Figure 10:** DC Bus Voltage, Current and Battery

Figure 10 illustrates the DC bus voltage, current and battery current. The dc bus voltage is stable, despite a current drop from approximately 200 A to 50 A, as shown in Figure 10. The dc bus is current and also stables. As is clear, the battery current is positive, and the generator supplies power to the battery and UC modules. This suggests that the MG modules are charging and the voltage starts increasing from the initial value of 5V.

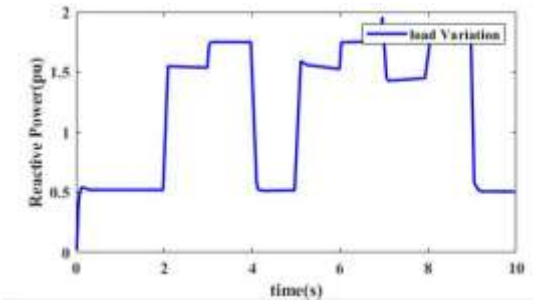


**Figure 11:** Reactive Power Load Variation

Figure 11 depicts the reactive power load variation. It depicts that the primary reactive load is o.5 pu before 1s. These figures depict that the proposed droop control approach stabilizes the MG voltage and frequency following the step load changes. The frequency following the step load changes.

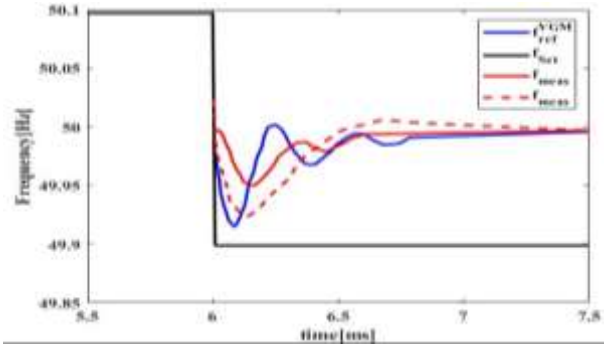


**Figure 12:** Frequency of Droop Strategy

As shown in Figure 12, when the load is connected in 0.4 s, the droop control strategy frequency curve decreases rapidly, while the frequency curve of the VSG control strategy decreases to the same frequency at about 0.6 s due to the existence of inertia. In addition, the frequency curve of the droop control strategy rises rapidly when the load is cut off in 0.8 s, while the proposed control strategy returns to stability at 1s. It can be seen that compared with droop control, can alleviate the impact on the system during load switching.

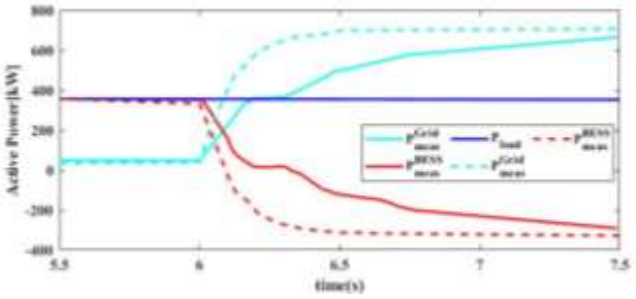


**Figure 13:** Active Power in Different Sources

Figure 13 shows that the calculated active power is close to the simulated one. This exemplifies the total active power of the grid and BESS. Further, the average value of total active power per 7.5s is considered as dispatch order. Parameters of the controlling strategy, which are mentioned in this paper are as follows: the long controlling period is 1 min and the short controlling period is 5.5s;

### 5.1 Case Study Analysis with Different Load Conditions

This section of the proposed study deals with justifying the supremacy of the proposed Mamdani Fuzzy Type II PID controller technique over the original Type I and Type III algorithm under different uncertainties conditions of the MG system. Regarding this, the LFC study due to various uncertainties is demonstrated through different scenarios.

**Case Study 1:** Variation of only load (ΔPL) In this case study to obtain the LFC of an interconnected MG system a random pattern load (RLP) as shown in Figure 14 is affected in area 1 at time t=0 while affected disturbances of wind and solar power are zero. Concerning this disturbance, the deviated responses of frequency and tie-line power resulted due to different techniques optimized type-II fuzzy PID controller are depicted in this section. To obtain simulated dynamic responses, the optimal gain parameters of the type-II fuzzy controller due to different techniques along with respective ITAE values are gathered.

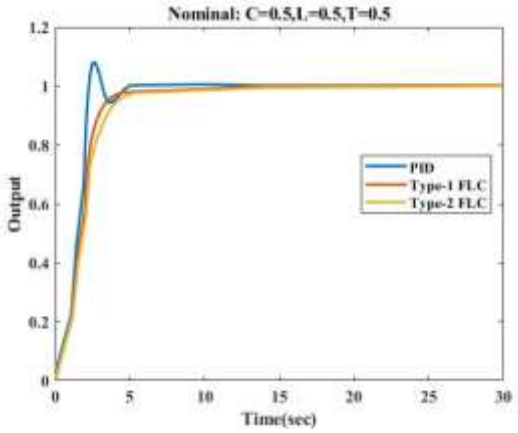


**Figure 14:** Dynamic Responses Obtained Via Fuzzy Controller

From figure 14, both the type-1 and type-2 fuzzy logic controllers outperform the conventional PID controller in terms of overshoot. The conventional PID controller performs better concerning rise-time and integral of absolute error (IAE). The type-1 FLC performs better than the type-2 FLC in terms of rise-time, settling-time, and IAE. Further, improve the fuzzy logic controller outputs using a Mamdani type FIS since it also provides lower MF scale and lag parameters for output membership functions. However, a Mamdani type-2 FLC introduces additional computational delay due to the expensive type-reduction process.

**Case Study 2:** Fluctuation in solar irradiation power only, ΔPL=0, ΔPL=0. In this scenario, a solar irradiation power fluctuation signal shown in Figure 15 is affected at area1 at time t=0.5s. Critical analysis confers our proposed algorithm exhibits superior performance over other implemented techniques regarding settling time; peak overshoot and peak undershoot of all resulting from dynamic responses

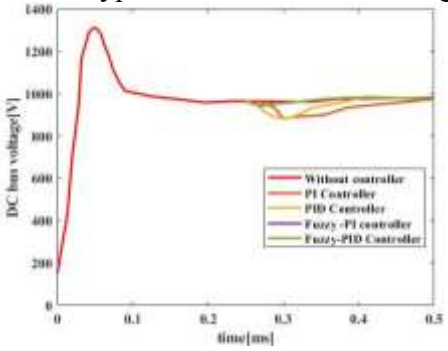


**Figure 15:** DC Bus Voltage with Solar Load

According to figure 15, the dynamic responses have been depicted through different conditions revealing that the proposed I-PI optimized type-II fuzzy PID controller exhibits more effectiveness over other techniques based proposed type-II fuzzy controller. This concludes that responses obtained due to Fuzzy PI optimized type-II fuzzy PID controller exhibits the least settling time, minimal peak overshoot and undershoot.

**Case Study 3:** Fluctuation in wind power only (ΔPW), ΔPL=0, ΔPϕ=0 for this study a wind power fluctuation signal shown in Figure 16 is affected at area1 at time t=0. All deviated responses due to different optimization techniques based on type-II fuzzy PID controller.

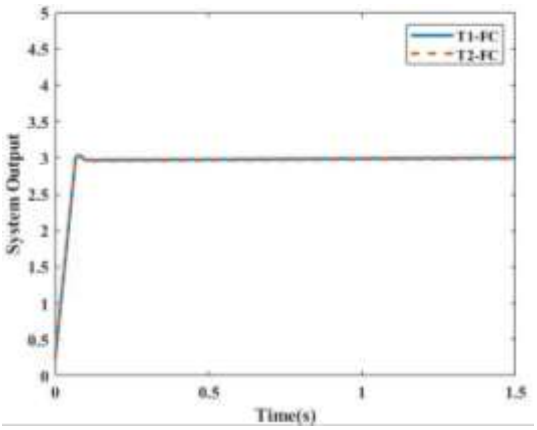


**Figure 16:** T1 and T2 System Output

According to Figure 16, it has been noticed through different dynamic responses that the proposed technique is more effective than TI, and T2 techniques in the LFC study of interconnected MG systems. Output from the controller Fuzzy-II/Fuzzy-III will have to provide the best results while also ensuring minimal DER operation for the desired power demand.

## 6. Research Conclusion

Microgrids (MGs) are designed with the help of effective power extracted from renewable sources such as solar, wind, battery, and biomass. The hybrid AC/DC microgrid consists of both AC and DC grids tied by an Interlinking Converter (ILC). It comprises a DC grid and AC grid interlinked by a bidirectional DC/AC converter. Lithium-ion batteries were chosen for this study due to their high energy density, long life cycle, and high efficiency. Multi-Input Booster (MIB) DC-DC converters are being used as a power converter in between load and source to enforce and increase the PV depending on the voltage output signal. AC microgrids are based on the ILC droop control coefficients of sources to transfer power from DC microgrid to AC microgrid. The voltage and frequency of MGs are strongly impressionable from the active and reactive load fluctuations. Mamdani type 2 PID-fuzzy controller into the high-type control system, exhibits high performance and desirable response for different scenarios of change in load. This proposed control strategy successfully reduced the renewable fluctuations in the microgrid.

Simulations are carried out in the Matlab/Simulink software. The results show that the interlink converter improves the flexibility of the hybrid microgrid and, in addition, the power quality of the energy supplied in the utility grid is improved. The system elaborated here always tends to keep the battery's state of charge (SOC) above 90%. Additionally, a sensitivity analysis was performed to report the impact of cost variations. These results prove that it is possible to satisfy the electrical demand of rural communities at a reasonable and accessible cost. This research demonstrates that the fuzzy-PID controller is a good alternative for controlling power converters and non-linear systems. The performance and properties of the proposed optimized charging control system are evaluated using a three-simulation case study. The security analysis of this framework is evaluated using some indices. In this approach, two well-known performance indices, including Power Performance Index (PIP) and Voltage Performance Index (PIV), are used to analyze the electrical networks' security.

*References*

[1] Dawoud, S., 2022. Economic and Environmental Investigation of

Renewable Energy Sources for Micro-grids coastal areas. Journal of Engineering Research, 6(1), pp.91-97.

[2] Goudarzi, A., Li, Y. and Xiang, J., 2021. Efficient energy management of renewable resources in microgrids. In Renewable Energy Microgeneration Systems (pp. 285-321). Academic Press.

[3] Kharrich, M., Kamel, S., Abdeen, M., Mohammed, O.H., Akherraz, M., Khurshaid, T. and Rhee, S.B., 2021. Developed approach based on equilibrium optimizer for optimal design of hybrid PV/Wind/Diesel/Battery microgrid in Dakhla, Morocco. IEEE Access, 9, pp.13655-13670.

[4] Albarakati, A.J., Boujoudar, Y., Azeroual, M., Jabeur, R., Aljarbouh, A., El Moussaoui, H., Lamhamdi, T. and Ouaaline, N., 2021. Real-time energy management for DC microgrids using artificial intelligence. Energies, 14(17), p.5307.

[5] Sharma, R. and Bhatt, P.K., 2022. Optimal Design Analysis of Multimodal Hybrid AC/DC Microgrids. Mathematical Statistician and Engineering Applications, 71(2), pp.138-150.

[6] Bouchekara, H.R.E.H., Javaid, M.S., Shaaban, Y.A., Shahriar, M.S., Ramli, M.A.M. and Latreche, Y., 2021. Decomposition based multiobjective evolutionary algorithm for PV/Wind/Diesel Hybrid Microgrid System design considering load uncertainty. Energy Reports, 7, pp.52-69.

[7] Gamil, M.M., Senjyu, T., Masrur, H., Takahashi, H. and Lotfy, M.E., 2022. Controlled V2Gs and battery integration into residential microgrids: Economic and environmental impacts. Energy Conversion and Management, 253, p.115171.

[8] Gui, Y., Han, R., Guerrero, J.M., Vasquez, J.C., Wei, B. and Kim, W., 2021. Large-Signal stability improvement of DC-DC converters in DC microgrid. IEEE Transactions on Energy Conversion, 36(3), pp.2534-2544.

[9] Armghan, A., Azeem, M.K., Armghan, H., Yang, M., Alenezi, F. and Hassan, M., 2021. Dynamical Operation Based Robust Nonlinear Control of DC Microgrid Considering Renewable Energy Integration. Energies, 14(13), p.3988.

[10] Albalawi, H., El-Shimy, M.E., AbdelMeguid, H., Kassem, A.M. and Zaid, S.A., 2022. Analysis of a Hybrid Wind/Photovoltaic Energy System Controlled by Brain Emotional Learning-Based Intelligent Controller. Sustainability, 14(8), p.4775.

[11] Jabeur, R., Boujoudar, Y., Azeroual, M., Aljarbouh, A. and Ouaaline, N., 2022. Microgrid energy management system for smart home using multi-agent system. International Journal of Electrical & Computer Engineering (2088- 8708), 12(2).

[12] Kumar, N.K., Gopi, R.S., Kuppusamy, R., Nikolovski, S., Teekaraman, Y., Vairavasundaram, I. and Venkateswarulu, S., 2022. Fuzzy Logic-Based Load Frequency Control in an Island Hybrid Power System Model Using Artificial Bee Colony Optimization. Energies, 15(6), p.2199.

[13] Arrar, S. and Xioaning, L., 2022. Energy Management in Hybrid Microgrid using Artificial Neural Network, PID, and Fuzzy Logic Controllers. European Journal of Electrical Engineering and Computer Science, 6(2), pp.38-47.

[14] Al Sumarmad, K.A., Sulaiman, N., Wahab, N.I.A. and Hizam, H., 2022. Energy Management and Voltage Control in Microgrids Using Artificial Neural Networks, PID, and Fuzzy Logic Controllers. Energies, 15(1), p.303.

[15] Kaysal, A., Köroğlu, S. and Yüksel, O.Ğ.U.Z., Self-tuning Fuzzy PID Controller Design and Energy Management in DC Microgrid: Standalone and Grid Connected Mode. Celal Bayar University Journal of Science, 18(1), pp.41-51.

[16] Tarife, R., Nakanishi, Y., Chen, Y., Zhou, Y., Estoperez, N. and Tahud, A., 2022. Optimization of Hybrid Renewable Energy Microgrid for Rural Agricultural Area in Southern Philippines. Energies, 15(6), p.2251.

[17] Punna, S., Mailugundla, R. and Salkuti, S.R., 2022. Design, Analysis and Implementation of Bidirectional DC–DC Converters for HESS in DC Microgrid Applications. Smart Cities, 5(2), pp.433-454.

[18] Doshi, K. and Harish, V.S.K.V., 2021. Analysis of a wind-PV battery hybrid renewable energy system for a dc microgrid. Materials Today: Proceedings, 46, pp.5451-5457.

[19] Ullah, Z., Elkadeem, M.R., Kotb, K.M., Taha, I.B. and Wang, S., 2021. Multi-criteria decision-making model for optimal planning of on/off grid hybrid solar, wind, hydro, biomass clean electricity supply. Renewable Energy, 179, pp.885-910.

[20] Suman, G.K., Guerrero, J.M. and Roy, O.P., 2021. Optimisation of solar/wind/bio-generator/diesel/battery based microgrids for rural areas: A PSO-GWO approach. Sustainable cities and society, 67, p.102723.

[21] Allouhi, A., Rehman, S. and Krarti, M., 2021. Role of energy efficiency measures and hybrid PV/biomass power generation in designing 100% electric rural houses: A case study in Morocco. Energy and Buildings, 236, p.110770.

[22] Zeng, J., Du, X. and Yang, Z., 2021. A Multiport Bidirectional DC–DC Converter for Hybrid Renewable Energy System Integration. IEEE Transactions on Power Electronics, 36(11), pp.12281-12291.

[23] Fathy, A., Alanazi, T.M., Rezk, H. and Yousri, D., 2022. Optimal energy management of micro-grid using sparrow search algorithm. Energy Reports, 8, pp.758-773.

[24] Aryan Nezhad, M., 2022. Frequency Control and Power Balancing in a Hybrid Renewable Energy System (HRES): Effective Tuning of PI Controllers in the Secondary Control Level. Journal of Solar Energy Research, 7(1), pp.963-970.

[25] Elkasem, A.H., Khamies, M., Magdy, G., Taha, I. and Kamel, S., 2021. Frequency Stability of AC/DC Interconnected Power Systems with Wind Energy Using Arithmetic Optimization Algorithm-Based Fuzzy-PID Controller. Sustainability, 13(21), p.12095.

**Contribution of Individual Authors to the Creation of a Scientific Article (Ghostwriting Policy)**

The authors equally contributed in the present research, at all stages from the formulation of the problem to the final findings and solution.

**Sources of Funding for Research Presented in a Scientific Article or Scientific Article Itself**

No funding was received for conducting this study.

**Conflict of Interest**

The authors have no conflicts of interest to declare that are relevant to the content of this article.